# Role of Metal Contacts in High-Performance Phototransistors Based on WSe$_2$ Monolayers

Wenjing Zhang,[†,§,||] Ming-Hui Chiu,[⊥] Chang-Hsiao Chen,[‡] Wei Chen,[§,#] Lain-Jong Li,[‡,⊥,*] and Andrew Thye Shen Wee[§,*]

[†]SZU-NUS Collaborative Innovation Center for Optoelectronic Science & Technology, Shenzhen University, Shenzhen 518060, China, [‡]Institute of Atomic and Molecular Sciences, Academia Sinica, Taipei, 11529, Taiwan, [§]Department of Physics, National University of Singapore, 2 Science Drive 3, Singapore 117542, [⊥]Physical Sciences and Engineering, King Abdullah University of Science and Technology, Thuwal, 23955-6900 Kingdom of Saudi Arabia, [||]Key Laboratory of Optoelectronic Devices and Systems of Ministry of Education and Guangdong Province, Shenzhen University, Shenzhen 518060, China, and [#]Department of Chemistry, National University of Singapore, 3 Science Drive 3, Singapore 117543

ABSTRACT Phototransistors based on monolayer transition metal dichalcogenides (TMD) have high photosensitivity due to their direct band gap transition. However, there is a lack of understanding of the effect of metal contacts on the performance of atomically thin TMD phototransistors. Here, we fabricate phototransistors based on large-area chemical vapor deposition (CVD) tungsten diselenide (WSe$_2$) monolayers contacted with the metals of different work function values. We found that the low Schottky-contact WSe$_2$ phototransistors exhibit a very high photo gain (10^5)

and specific detectivity (10^{14} Jones), values higher than commercial Si- and InGaAs-based photodetectors; however, the response speed is longer than 5 s in ambient air. In contrast, the high Schottky-contact phototransistors display a fast response time shorter than 23 ms, but the photo gain and specific detectivity decrease by several orders of magnitude. Moreover, the fast response speed of the high Schottky-contact devices is maintained for a few months in ambient air. This study demonstrates that the contact plays an important role in TMD phototransistors, and barrier height tuning is critical for optimizing the photoresponse and photoresponsivity.
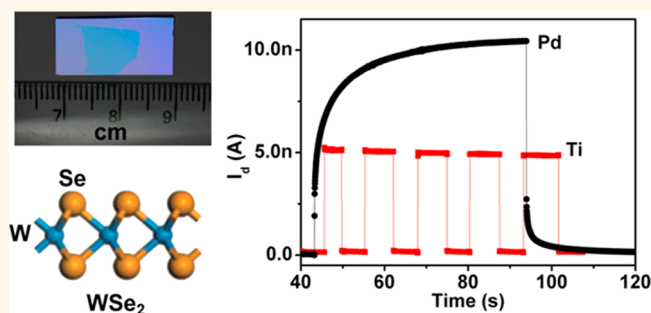
KEYWORDS: photodetector · contact effect · Schottky barrier · tungsten diselenide · 2D material

The monolayer two-dimensional (2D) transition metal dichalcogenides (TMDs) are potentially important building blocks for nanoscale optoelectronics due to their unique optical properties.[1−9] Recently, there has been much interest in the molybdenum disulfide (MoS$_2$) monolayer because of its direct band gap of ∼1.8 eV,[10] excellent ON/OFF current ratio of 10^8,[11] high photo gain of 5000,[12] and high specific detectivity of $10^{10}−10^{11}$ Jones.[13] However, the response time of the reported MoS$_2$ phototransistors for either exfoliated or CVD synthesized MoS$_2$ varies from <1 ms to >30 s.[2,12−16] Distinctly different photoresponse behaviors at the ON state of MoS$_2$ phototransistors have also been observed. Kim *et al.* found that there was no photocurrent at the ON state.[13,16] In contrast, Kis *et al.* presented a high photocurrent at the ON state for MoS$_2$ phototransistors.[2,12,14]

In addition, most of these groups attributed the photocurrent to the separation of photo-generated electron−hole pairs at the metal/semiconductor interface.[2,12−16] However, Castellanos-Gomez's group claimed that the photocurrent is dominated by the photothermoelectric effect for their ohmic-contact MoS$_2$ phototransistors.[17,18] The Schottky contact between semiconducting channels and metallic electrodes plays an important role for a conventional photodetector based on the metal−semiconductor-metal structure.[19] Many groups tentatively attributed the different electrical and optical transport properties to the Schottky contacts.[2,12−18] However, there is still no systematic research on the role of the metal contact in photodetectors based on atomically thin TMD layer materials.

As MoS$_2$ films on SiO$_2$/Si substrates are heavily n-doped by defects, charged

impurities and adsorbates, it is difficult to tune the Schottky barrier height at the interface between MoS_2 channels and metallic electrodes.[20,21] Nevertheless, we have recently synthesized highly quality crystalline and large-area tungsten diselenide (WSe_2) monolayers on sapphire by the CVD method,[22] and successfully transferred the monolayer WSe_2 films to SiO_2/Si substrates. The monolayer films display strong photoluminescence, opening up potential applications in optoelectronics. Using the transferred CVD WSe_2 monolayer films as channels, we fabricate monolayer WSe_2 transistors and systematically study the Schottky contact effect on the electrical and optical transport properties of atomically thin TMD materials. We demonstrate low Schottky barrier p-type transistors with an ON/OFF current ratio of up to 10^9 and mobility larger than 7.3 cm^2/(V s) using high work function Pd metal contacts. The external photo gain of the Pd-contacted monolayer WSe_2 device is up to 3.5×10^5 and the specific detectivity is higher than 10^{14} Jones. However, the photocurrents for the Pd-contacted devices take more than 5 s to saturate in ambient air. In contrast, the high Schottky-barrier WSe_2 devices using low work function Ti metal contacts present a much faster response time of <23 ms, and better photocurrent linearity as a function of incident optical power. We suggest a qualitative mechanism based on metal/semiconductor junction energy band diagrams to explain these distinctly different phenomena.

RESULTS AND DISCUSSION

The large area WSe_2 monolayers were grown on sapphire by the vapor-phase reaction of WO_3 and Se powders in a hot-wall CVD chamber as described in our previous work.[22] After growth, the films were transferred to 300 nm SiO_2/Si substrates. Figure 1a shows the optical image of a $\sim1 \times 1$ cm transferred film on SiO_2/Si substrate, and Figure 1b is the magnified optical image with no obvious optical contrast difference across the field, indicating that the transferred film was uniform.[23] Atomic force microscopy (AFM), Raman spectroscopy, and photoluminescence (PL) were used to characterize the number of layers and quality of the transferred films. As shown in Figures 1c,d, the representative thickness of the transferred films is ~0.97 nm, which is slightly thicker than the as-grown monolayer WSe_2 on SiO_2/Si,[22,24,25] and this could be attributed to residual chemical contamination of the transferred process or the substrate effect.[26] The Raman spectra for the transferred films excited by a 473 nm laser are shown in Figure 1e, where two characteristic peaks at 248 and 259 cm^{-1} are observed. According to the calculated phonon dispersion and experimental studies of monolayer WSe_2, the peak at 248 cm^{-1} is assigned to the in-plane vibrational E_{2g}^1 mode.[27−32] However, there are different assignments in the literature for the peak at ~259 cm^{-1}. Some papers attributed it to the out-of-plane A_{1g} mode,[27−29] while others assign it to second order longitudinal acoustic phonons at the M point (2LA(M)) in the Brillouin zone.[30,31] Regardless of assignment, the Raman spectra of our transferred films are consistent with those of mechanically exfoliated natural WSe_2 monolayers. In addition, the strong PL of the WSe_2 film implies a highly radiative recombination rate, in agreement with the direct band transition for the WSe_2 monolayer. The typical peak position of the PL spectrum is ~763 nm, corresponding to a band gap of ~1.63 eV.[32] All optical images, AFM, Raman and PL spectra confirm that the transferred film is high-quality WSe_2 monolayer.
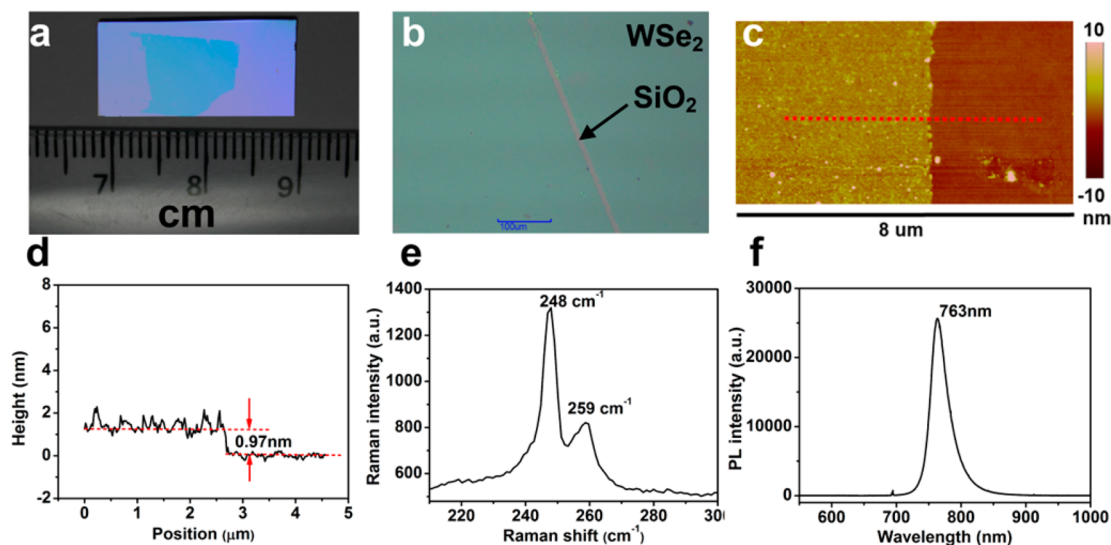

Figure 1. Characterization of the transferred CVD monolayer WSe_2. (a and b) The optical image of transferred CVD monolayer WSe_2 on SiO_2/Si substrate. (c) The AFM image at the edge of the monolayer film. (d) The height profile along the dotted red line in (c). (e and f) The typical Raman and photoluminescence spectra of the transferred film, respectively.
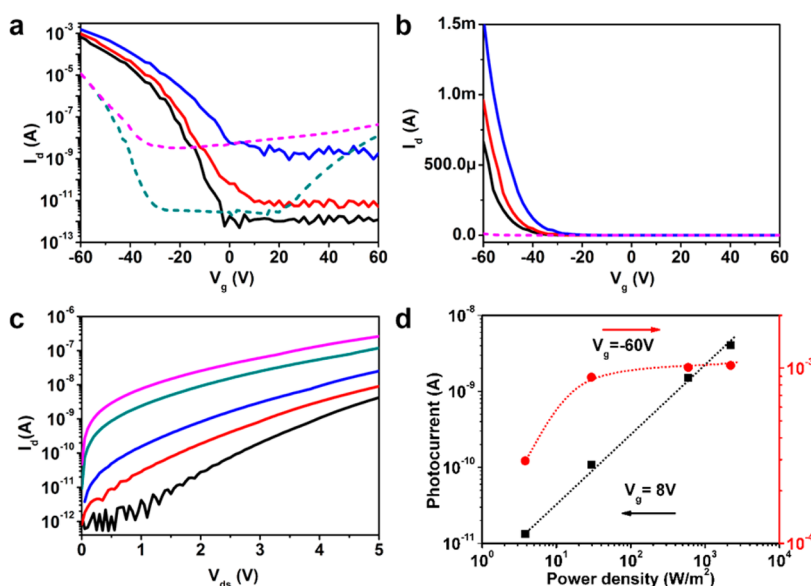
Figure 2. Optoelectrical properties of the CVD monolayer WSe$_2$ phototransistor in ambient and vacuum with Pd metal contacts. (a and b) I_d–V_g transfer characteristics of the transistor on a logarithmic and linear scale, respectively, in dark and at the laser power density 3.8 and 0.22 W/cm^2 and V_{ds} = 2 V. The measured conditions are dark in ambient (black solid), 3.8 W/m^2 light in ambient (red solid), 0.22 W/cm^2 light in ambient (blue solid), dark in vacuum (dark cyan short dash), and 0.22 W/cm^2 light in vacuum (magenta short dash). (c) I_d–V_{ds} characteristics of the transistor as a function of light intensity on a logarithmic scale, at V_g = 0 V. From bottom to top, the curves are measured at the following intensities: in dark (black), 3.8 W/m^2 (red), 59.5 W/m^2 (blue), 595.3 W/m^2 (dark cyan), and 0.22 W/cm^2 (magenta). (d) The power dependence of the photocurrent at V_g = 8 V (OFF-state) and V_g = −60 V(ON-state).

After the transfer and characterization of the WSe$_2$ monolayer, standard photolithography was applied to fabricate WSe$_2$ transistors. Supporting Information Figure S1 shows the device structure and optical photograph of the phototransistor, where the 10/80 nm Ti/Au or 10/80 nm Pd/Au interdigitated electrodes are deposited by thermal evaporation, respectively, to form two types of metal−semiconductor−metal (MSM) structures: high Schottky-contact and low Schottky-contact based photodetector devices. All of the electrical and optical properties were measured at room temperature.

We first present the electrical transport properties of the CVD monolayer WSe$_2$ transistor with Pd metal contacts, where the work function of Pd is much higher than that of the WSe$_2$ monolayer.[24] As depicted in the back-gate transfer characteristics in Figure 2a,b, the Pd-contacted transistor exhibits obvious p-type conduction, and the threshold voltage is ~0 V in ambient air. The unipolar p-type behavior of the Pd-contacted photodetector suggests that the Fermi level is aligned close to the valence band of the monolayer WSe$_2$.[24,33−35] The maximum transconductance is $g_m = dI_d/dV_g$ = 84.9 μS at V_{ds} = 2 V in the measurement gate voltage range, and the subthreshold swing is $S = dV_g/d(\log I_d)$ = 283 mV/decade in our bottom gate structure. According to the standard model of metal-oxide-semiconductor field effect transistors and the parallel plate model of gate capacitance, the hole mobility $\mu = g_mL/(WC_{ox}V_{ds})$ is ~7.3 cm^2/(V s) in ambient air, where L is the channel length, W is the channel width, V_{ds} is the drain voltage, and C_{ox} is the capacitance of the 300 nm SiO$_2$. The ON/OFF current

ratio of the Pd-contacted transistor is up to an impressive value of ~10^9, and the dark current is ~10^{-12}A in the OFF state.

To evaluate the performance of the photodetector, the light power density (P_0) dependence of the photocurrent is studied with a continuous wavelength 650 nm laser illumination in ambient air with spot size of ~1 mm. The high sensitivity of the photodetector can be seen in Figure 2c, where the current is reversibly varied between 1 to 4 orders of magnitude by changing the light intensity from 3.8 to 0.22 W/cm^2. As shown in Figure 2d, the photocurrent ($I_{ph} = I_{illumination} - I_{dark}$) increases almost linearly with light power density ($I_{ph} \sim P_0^{0.91}$) in the OFF state at V_g = 8 V, V_{ds} = 2 V, demonstrating the efficiency of electron−hole pair generations is almost proportional to the absorbed photon flux.[12] However, the photocurrent becomes significantly sublinear with light power density in the ON state (at V_g = −60 V, V_{ds} = 2 V; red curve in Figure 2d), indicating that the recombination of photoexcited electron−hole pairs becomes pronounced, or a different photocurrent-generated mechanism occurs in the ON state.[12,18,36,37] To quantitatively define the performance of the photodetector, we extract the photo responsivity and photo gain of the device (Figure 3a,b). For the OFF state (V_g = 8 V, V_{ds} = 2 V and P_0 = 3.8 W/m^2) in ambient air, the photo responsivity $R = I_{ph}/P$ is ~0.008 A/W, where P is the absorbed laser power, and the photo gain $G = Rh\nu/\eta q$ is ~0.016 assuming that η = 100%, where h is the Planck constant, ν is the frequency of the incident laser, η is the external quantum efficiency,
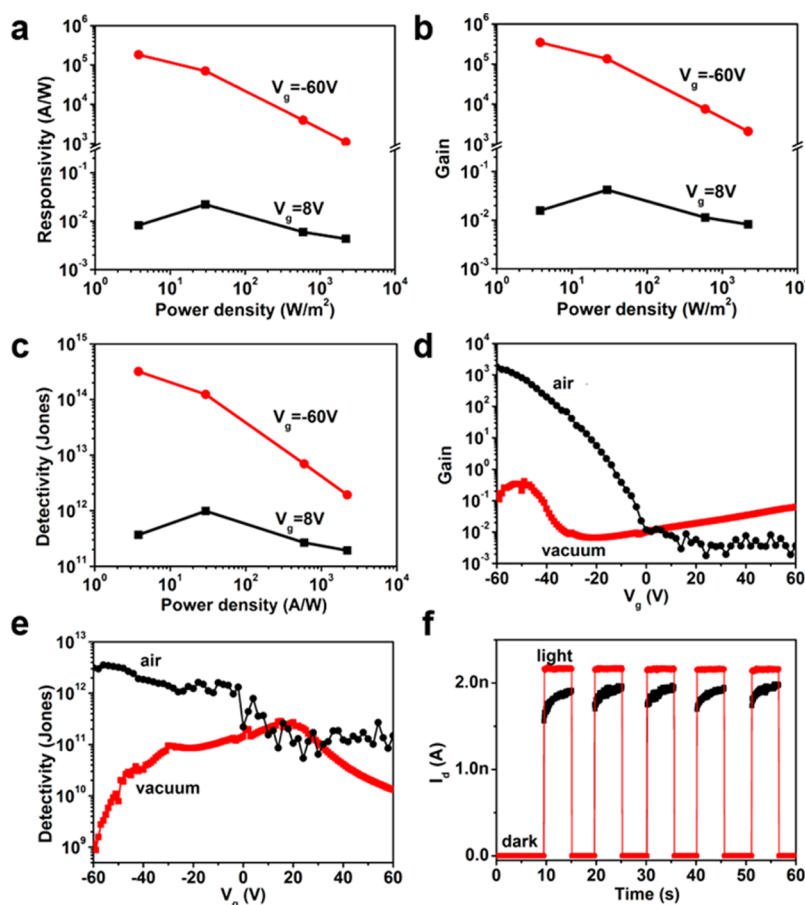
Figure 3. Performance of the phototransistor based on CVD WSe$_2$ monolayer with Pd metal contacts. (a−c) The light power density dependence of the photo responsivity, photo gain, and specific detectivity, respectively. (d and e) The photo gain and specific detectivity of the photodetector in ambient air and vacuum at laser power density 0.22 W/cm^2 and $V_{ds} = 2$ V. (f) The time-resolved photoresponse of the device in ambient (black) and vacuum (red) at $V_{ds} = 2$ V, $V_g = 0$ V, $P_0 = 170$ W/m^2.

and q is the electron charge.[38] Interestingly, the photo responsivity and gain of the photodetector in ambient drastically increase to ∼1.8 × 10^5 A/W, and 3.5 × 10^5, respectively, in the ON state($V_g = -60$ V, $V_{ds} = 2$ V and $P_0 = 3.8$ W/m^2). The values of photo responsivity and gain obtained are much higher than those of commercial silicon and InGaAs photodetectors.[13,39−41] Specific detectivity is another figure of merit for photodetectors, which is related to the sensitivity that a detector can distinguish from the background noise. The shot noise from the dark current is assumed to be the major contributor to the total noise and the specific detectivity given by $D^* = RA^{1/2}/(2qI_d)^{1/2}$,[13] where R is the photoresponsivity, A is the area of the detector, q is the unit of charge, and I_d is the dark current. As shown in Figure 3c, D^* in the ON state is higher than 10^{14} Jones in ambient air at $V_g = -60$ V, $V_{ds} = 2$ V and $P_0 = 3.8$ W/m^2. The value is higher than that of commercial silicon (∼10^{13} Jones) or InGaAs (10^{12}−10^{13} Jones) photodetectors.[13,39−41] Even for the ON state at a high power density of $P_0 = 0.22$ W/cm^2 in ambient air, D^* is still >10^{12} Jones, which is comparable to commercial silicon and InGaAs photodetectors. In the OFF state at $V_g = 8$ V and $V_{ds} = 2$ V, the photodetector exhibits stable and good specific detectivity around 10^{11}−10^{12} Jones with light power density from 3.8 to 0.22 W/cm^2. The different photoresponse behaviors in ON and OFF states suggest that various mechanisms are at work.[12,18,36,37]

We have also studied the photoresponse properties of the WSe$_2$ monolayer phototransistor in high vacuum. As shown in Figure 2a, after vacuum pumping to 3.5 × 10^{-5} mbarr, the p-channel threshold voltage of the device shifts from 0 to −27 V, and the n-channel begins to conduct. The device becomes ambipolar, which means that the ambient adsorbates withdraw electrons from WSe$_2$, resulting in apparent p-doping of the WSe$_2$ monolayer device.[12] The Fermi level of WSe$_2$ moves from close to the valence band to nearer the midgap; thus, the Schottky barrier at the interface between the metallic electrodes and WSe$_2$ monolayer is higher in vacuum than in ambient air. When illuminating with the CW 650 nm laser at $P_0 = 0.22$ W/cm^2 and $V_{ds} = 2$ V, the current in the OFF state increases more than 3 orders of magnitude (Figures 2ab); however, the accumulation current in the ON state does not increase with the incident light, in sharp contrast to that in ambient air. Figure 3d,e compares the performance of the phototransistor in ambient air and high
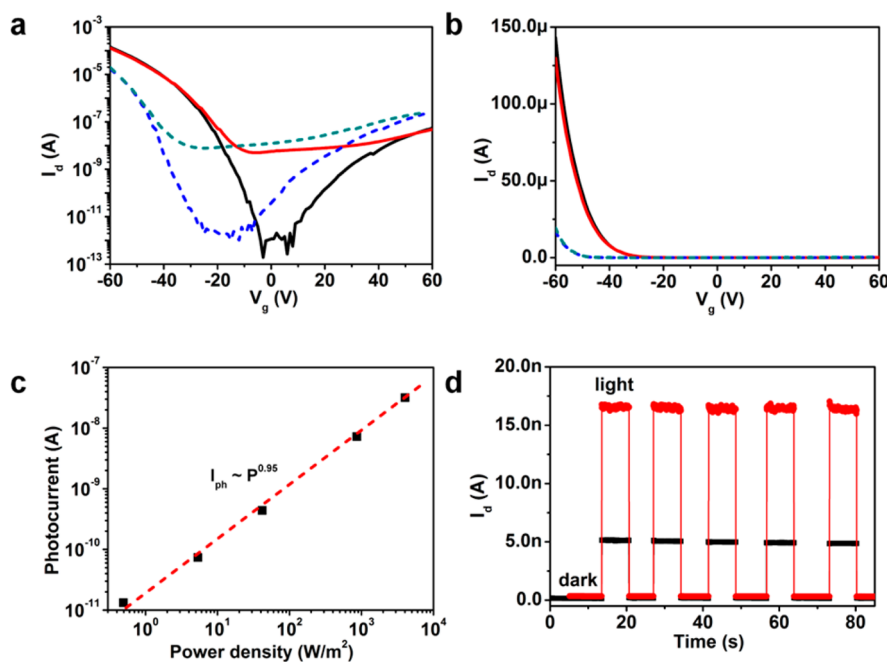
Figure 4. Room temperature photoresponse of the CVD monolayer WSe_2 phototransistor with Ti metal contacts. (a and b) I_d-V_g transfer characteristics of the photodetector on a logarithmic and linear scale, respectively, in dark and at the laser power density 0.4 W/cm^2, $V_{ds} = 2$ V. The measured conditions are dark in ambient (black solid), light in ambient (red solid), dark in vacuum (blue short dash), and light in vacuum (dark cyan short dash). (c) The laser power dependence of the photocurrent at $V_{ds} = 2$ V and $V_g = 0$ V. (d) The time-resolved photoresponse of the device in ambient (black) and vacuum (red) at $V_{ds} = 2$ V, $V_g = 0$ V, $P_0 = 0.4$ W/cm^2.

vacuum, and it can be seen that the photo gain and specific detectivity in the OFF states are almost the same, while both the photo gain and specific detectivity in the ON states decrease by more than 3 orders of magnitude from ambient to high vacuum. It has been suggested that, in the OFF state, the Schottky barrier is so high that the thermionic and tunneling currents are negligible, and the photogenerated current is the dominant channel current under illumination.[13,14,18] In the ON state, the movement of the Fermi level and the bending of energy band by the applied gate electric field result in the Schottky barrier height decrease; hence in this case the thermionic and tunneling currents dominate the channel current. For the Pd-contacted WSe_2 phototransistor in the ON state (*cf.* panels a and b in Figure 2), the photogenerated current is negligible in high vacuum. In contrast, the photogenerated current is very high in ambient, resulting in high photo gain and specific detectivity. These different photoresponse properties are attributed to the desorption of adsorbates in ambient air, causing the Fermi level of the WSe_2 monolayer to move toward the minimum of the conduction band and increase the Schottky barrier height at the electrode/WSe_2 interface.[42,43]

To verify that the Schottky barrier plays an important role, we fabricate monolayer WSe_2 photodetectors contacted with Ti, whose work function is close to that of WSe_2.[24] Figure 4 and Supporting Information Figure S2 present the electrical and photoresponse properties of the device. In Figure 4a, the Ti-contacted

phototransistor exhibits ambipolar behavior in ambient, and the threshold voltages in p and n channels are −2 and 8 V, respectively, indicating that the Fermi level of the WSe_2 monolayer is close to the midgap, and the Schottky barrier in the p channel is much higher than that with Pd metal contacts (Supporting Information Figure S3).[33−35] In high vacuum, the threshold voltages shift to negative voltages, consistent with the Pd-contacted device. The Fermi level moves to the minimum of the conduction band, resulting in an increase of the Schottky barrier in the p channel. As expected, with the increase of the Schottky barrier for the Ti-contacted WSe_2 photodetector in ambient, the channel current in the ON state does not change significantly under illumination (Figure 4a,b), similar to that for the Pd-contacted device in high vacuum, when the Fermi level is near the midgap. There is almost no photocurrent in the ON state for the Ti-contacted WSe_2 photodetector in ambient, which confirms that the increase of the Schottky barrier in the p channel results in the performance degradation of WSe_2 photodetection.

Normally, the Schottky barrier at the metal/semiconductor interface plays a crucial role in determining the optoelectronic transport property of the MSM structure.[44] At a fixed bias voltage, the voltage drop occurs mainly at the reverse biased Schottky barrier for the Schottky contact photodetector.[45−48] The photogenerated electron−hole pairs in the depletion region are separated by the strong local electric
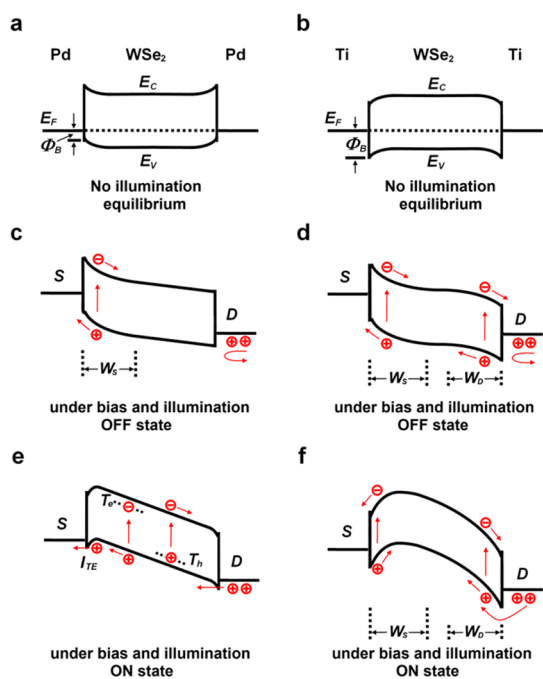
Figure 5. Energy band diagram of the photodetector based on the CVD WSe$_2$ monolayer. (a, c, and e) The band diagram of the device with Pd metal contacts in the equilibrium, OFF and ON state for hole carriers in the channel, respectively. (b, d, and f) The band diagram with Ti metal contacts in the equilibrium, OFF and ON state for hole carriers in the channel, respectively. E_F is the Fermi level energy, E_C is the minimum conduction band energy, E_V is the maximum valence band energy, and Φ_B is the Schottky barrier. In (e), I_{TE} indicates the photocurrent from the photo thermoelectric effect, T_e is the electron trapping state near to the minimum conduction band edge, and T_h is the hole trapping state near to the maximum valence band edge. W_S and W_D are the depletion regions at the source electrode/WSe$_2$ and drain electrode/WSe$_2$ interfaces, respectively. S and D indicate the source and drain electrodes, respectively. The source electrode is grounded and the drain electrode is applied with a positive voltage in the experiment.

field, thus reducing the electron–hole recombination rates and increasing the free carrier density. Theory and experiments have shown that in the depletion region at the interface between the metallic electrodes and the low dimensional material, the potential tail decays extremely slowly, and the depletion region due to the Schottky barrier can extend to several micrometers in the channel.[46,49] Once the Schottky barrier decreases, the width of the barrier decreases.[46] The depletion region with the ohmic-like contact can be narrow enough such that the voltage drop associated with adsorbates, defects or charge impurities becomes important.[46,48] Alternatively, the photothermoelectric effect may dominate the photocurrent.[18] As shown in Figure 5a, the Fermi level of the CVD WSe$_2$ monolayer is near the valence band after contacting with Pd metal electrodes. In the OFF state (Figure 5c), the Fermi level is near the midgap, and the Schottky barrier is so high that the depletion region can extend several micrometers into the WSe$_2$ monolayer channel due to the larger band gap of monolayer WSe$_2$ and the ~10 μm

channel length.[46,49] Thus, the long depletion region with high voltage drop can efficiently separate the photogenerated electron–hole pairs, resulting in the linear power dependence of the photocurrent and fast response time (Figures 3f and 4c,d).[50] In the ON state with the Pd-contacts (Figure 5e), the Fermi level is near the valence band, and the Schottky barrier is so small that the depletion width becomes very narrow,[46] and the photogenerated carriers in the depletion region could be negligible.[13,14] However, the voltage drop from adsorbates, defects or charge impurities in the channel become prominent.[46,48] Thus, photodesorption or photoexcitation through defect or charge impurity states to band edge may contribute to photocurrents in the ON state (Figure 2a),[42,46,51] or the photothermoelectric effect could generate the photocurrent for the majority carriers (holes) of the WSe$_2$ could easily diffuse into the electrodes to produce the photocurrent.[18,52] As shown in Figure 3f, the photocurrent for the Pd-contacted photodetector in ambient air takes more than 5 s to saturate, and the response time can be resolved into two parts: fast response of less than 50 ms, and slow response of longer than 5s. We attribute the fast response component to band-to-band excitation, and the slow response time to the desorption or excitation through defect or charge impurity states to the band edge,[12,42] or to the photothermoelectric effect.[18,52]

As the work function of Ti is close to that of the WSe$_2$ monolayer, the Fermi level alignment is near the midgap of WSe$_2$ after contacts are made (Figure 5b).[33−35] Thus, the Schottky barrier is much higher than that with Pd metal contacts. In the OFF state for the Ti-contacted transistors, as shown in Figure 5d, there are two depletion regions W_S and W_D, which are from the high Schottky barrier between the source/drain electrodes and the channel,[46,53] and the process of generating a photocurrent with the Ti metal contacts is almost the same as that with the Pd metal contacts. However, in the ON state, in order to bend the energy band for the high Schottky barrier, the applied gate voltages are so high that the energy band near the drain electrode is also bent upward, and two depletion regions are formed (Figure 5f),[46,53] one near the source electrode (W_S) and the other near the drain electrode (W_D). As shown in Figure 5f, the photocurrents from the two depletion regions almost disappear owing to the two opposite regions connecting, and the two depletion regions make the voltage drops of the adsorbates, defects or charge impurities in the channel negligible. The photothermoelectric effect could not generate the photocurrent for the high Schottky barrier blocking the holes in WSe$_2$ to diffuse into the electrodes. Hence, the thermionic and tunneling currents dominate the channel current. As shown in Figure 4, the hole electric field mobility of the Ti-contacted WSe$_2$ photodetector decreases to 2.43 cm^2/(V s), and the subthreshold swing
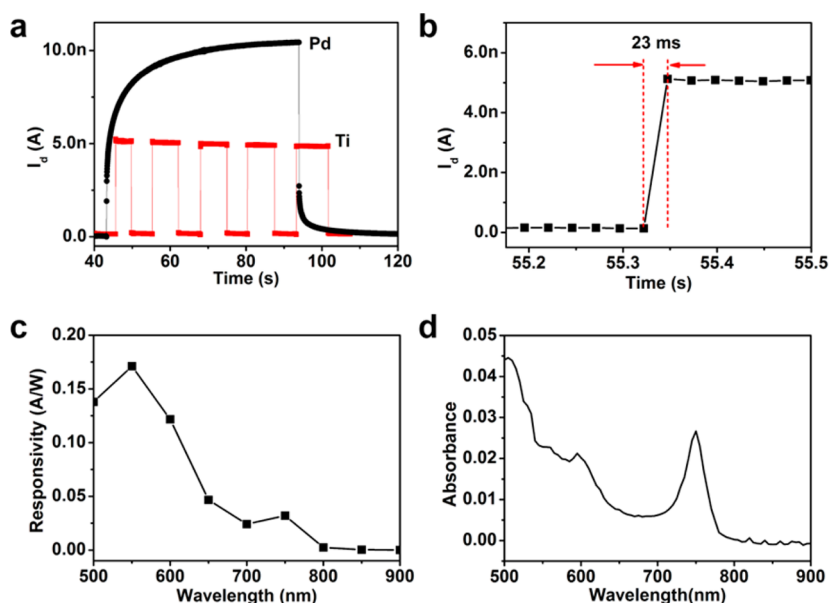
Figure 6. (a) Photoswitching behaviors of the Pd- and Ti-contacted photodetectors aged in ambient for one month. (b) Photoswitching rate of the photodetector with Ti metal contacts in ambient. The laser power density is 863 W/m^2, $V_{ds} = 2$ V and $V_g = 0$ V. (c) The wavelength dependence of the photo responsivity for the CVD monolayer WSe$_2$ photodetector at $V_{ds} = 2$ V, $V_g = 0$ V. (d) The absorbance spectrum of a CVD monolayer WSe$_2$.

for the p channel decreases to 320 mV/decade. Compared with the Pd-contacted photodetector, the photo gain and specific detectivity of the Ti-contacted photodetector decrease under the same experimental conditions (Supporting Information Figure S2c,d). The decrease in the mobility, subthreshold swing, photo gain and specific detectivity is attributed to the increase of the Schottky barrier height. However, the laser power dependence of the photocurrent becomes more linear, where $I_{ph} \sim P^{0.95}$, and only the fast part of the response time for the Ti-contacted photodetector in the ambient air is observed, which means that photothermoelectric generated photocurrents, photocurrents due to desorption or excitation through defect/charge impurity states to the band edge are not dominating factors. Interestingly, the response time of the Ti-contacted device remains less than 23 ms after one month in ambient air (Figures 6a,b), while the response time of the Pd-contacted device becomes much longer, which could be due to the movement of Fermi level further toward the valence band and the decrease of Schottky barrier height. In the Supporting Information (Figure S4), we present another typical Ti-contacted device which retains its performance even after aging for half a year.

The wavelength dependence of the photocurrent for the Ti-contacted WSe$_2$ phototransistor is shown in Figure 6c. The phototransistor exhibits good wavelength selectivity. When the light wavelength is shorter

than 800 nm, the responsivity is $\sim 10^{-4}$ A/W in the OFF state. It increases to 0.032 and 0.171 A/W under the 750 and 550 nm wavelength illumination, respectively. The profile of the wavelength dependence of the responsivity is consistent with the absorption spectrum (Figure 6d), indicating that the generated photocurrent is from the WSe$_2$ monolayer.

CONCLUSIONS

In conclusion, CVD monolayer WSe$_2$ phototransistors have been fabricated, and the Schottky contact effect on their optoelectronic properties has been investigated in detail. We propose a qualitative mechanism based on energy band bending at the metal/semiconductor junction to explain our observations. The phototransistor with Ti metal contacts exhibits fast photoresponse, where the rise and decay times are shorter than our detection limit, *i.e.*, 23 ms. Furthermore, the high performance remains stable even after half a year in ambient. These phototransistors based on the CVD WSe$_2$ monolayer are significantly better than those of CVD monolayer MoS$_2$ in terms of response time and material/device stability in ambient air. With its high photo gain, high detectivity, fast response speed, and high stability, the CVD monolayer WSe$_2$ phototransistors are demonstrated to display significant potential for future optoelectronic applications.

METHODS

Growth of Monolayer WSe$_2$. The WO$_3$ powders (0.3 g) were placed in a ceramic boat located in the heating zone center of

the furnace. The Se powders were placed in a separate ceramic boat at the upper stream side maintained at 270 °C during the reaction. The sapphire substrates for growing WSe$_2$ were put at

the downstream side, where the Se and WO_3 vapors were brought to the targeting sapphire substrates by an Ar/H_2 flowing gas (Ar = 80 sccm, H_2 = 20 sccm, chamber pressure = 1 Torr). The center heating zone was heated to 925 °C at a ramping rate of 25 C/min. Note that the temperature of the sapphire substrates was at ~750 to 850 °C when the center heating zone reaches 925 °C. After it reached 925 °C, the heating zone was kept for 15 min and the furnace was then naturally cooled to room temperature.

Transfer Process. An as-grown WSe_2 film was spin-coated by a layer of poly(methyl methacrylate) (PMMA), and baked at 100 °C for 1 h. Then, the PMMA-coated WSe_2 film was put into 2 M NaOH solution at 100 °C for 1 h, and subsequently, the PMMA-supported WSe_2 film was detached from sapphire substrate and floated on the surface of NaOH solution. Then, the floating PMMA-supported WSe_2 film was transferred to deionized (DI) water to remove the residual etchant, using SiO_2/Si substrate to fish up the PMMA-coated WSe_2 film, and followed with 100 °C drying for 30 min. Finally, the PMMA was removed by acetone, isopropyl alcohol (IPA) and DI water rinsing.

Device Fabrication. The phototransistors were fabricated on 300 nm SiO_2/Si substrate by standard photolithography. The 10/80 nm Ti/Au or 10/80 nm Pd/Au interdigitated electrodes are deposited by thermal evaporation, respectively, to form two types of metal−semiconductor−metal (MSM) structures. The as-fabricated devices were directly sent for electrical measurements without performing any thermal annealing.

Characterizations. The AFM images were obtained using a Veeco Dimension-Icon system. Raman and PL spectra were collected in a confocal Raman/PL system (NT-MDT). The wavelength of the laser was 473 nm (2.63 eV), and the spot size of the laser beam was ~0.5 μm. The spectral resolution was 3 cm^{-1} (obtained with a 600 grooves mm^{-1} grating). A high grating (1800 grooves mm^{-1}) was also used to obtain more details of the line shapes of the Raman band, and the spectral resolution was 1 cm^{-1}. The Si peak at 520 cm^{-1} was used as a reference for wavenumber calibration, and the peak frequency was extracted by fitting a Raman peak with a Lorentz function. The electrical measurements were performed under ambient or vacuum conditions using a Keithley semiconductor parameter analyzer, model 4200-SCS. A 650 nm laser was used to measure the photoresponse of the devices, and the spot size was ~1 mm.

Conflict of Interest: The authors declare no competing financial interest.

Supporting Information Available: The structure of phototransistors, performance of Ti-contacted devices, comparison of devices performance for different contact metals, and the performance of a typical Ti-contacted WSe_2 phototransistor half a year later. This material is available free of charge *via* the Internet at http://pubs.acs.org.

REFERENCES AND NOTES

1. Wang, Q. H.; Kalantar-Zadeh, K.; Kis, A.; Coleman, J. N.; Strano, M. S. Electronics and Optoelectronics of Two-dimensional Transition Metal Dichalcogenides. *Nat. Nanotechnol.* **2012**, *7*, 699–712.
2. Yin, Z.; Li, H.; Li, H.; Jiang, L.; Shi, Y.; Sun, Y.; Lu, G.; Zhang, Q.; Chen, X.; Zhang, H. Single-Layer MoS_2 Phototransistors. *ACS Nano* **2012**, *6*, 74–80.
3. Splendiani, A.; Sun, L.; Zhang, Y.; Li, T.; Kim, J.; Chim, C.; Galli, G.; Wang, F. Emerging Photoluminescence in Monolayer MoS_2. *Nano Lett.* **2010**, *10*, 1271–1275.
4. Eda, G.; Yamaguchi, H.; Voiry, D.; Fujita, T.; Chen, M.; Chhowalla, M. Photoluminescence from Chemically Exfoliated MoS_2. *Nano Lett.* **2011**, *11*, 5111–5116.
5. Zeng, H.; Dai, J.; Yao, W.; Xiao, D.; Cui, X. Valley Polarization in MoS_2 Monolayers by Optical Pumping. *Nat. Nanotechnol.* **2012**, *7*, 490–493.
6. Wu, S.; Ross, J. S.; Liu, G.-B.; Aivazian, G.; Jones, A.; Fei, Z.; Zhu, W.; Xiao, D.; Yao, W.; Cobden, D.; Xu, X. Electrical Tuning of Valley Magnetic Moment through Symmetry Control in Bilayer MoS_2. *Nat. Phys.* **2013**, *9*, 149–153.
7. Li, H.; Wu, J.; Yin, Z.; Zhang, H. Preparation and Applications of Mechanically Exfoliated Single-Layer and Multilayer MoS_2 and WSe_2 Nanosheets. *Acc. Chem. Res.* **2014**, *47*, 1067–1075.
8. Huang, X.; Tan, C.; Yin, Z.; Zhang, H. Hybrid Nanostructures Based on Two-Dimensional Nanomaterials. *Adv. Mater.* **2014**, *26*, 2185–2204.
9. Huang, X.; Zeng, Z.; Zhang, H. Metal Dichalcogenide Nanosheets: Preparation, Properties and Applications. *Chem. Soc. Rev.* **2013**, *42*, 1934–1946.
10. Mak, K. F.; Lee, C.; Hone, J.; Shan, J.; Heinz, T. F. Atomically Thin MoS_2: A New Direct-Gap Semiconductor. *Phys. Rev. Lett.* **2010**, *105*, 136805.
11. Radisavljevic, B.; Radenovic, A.; Brivio, J.; Giacometti, V.; Kis, A. Single-Layer MoS_2 Transistors. *Nat. Nanotechnol.* **2011**, *6*, 147–150.
12. Zhang, W.; Huang, J.-K.; Chen, C.-H.; Chang, Y.-H.; Cheng, Y.-J.; Li, L.-J. High-Gain Phototransistors Based on a CVD MoS_2 Monolayer. *Adv. Mater.* **2013**, *25*, 3456–3461.
13. Choi, W.; Cho, M. Y.; Konar, A.; Lee, J. H.; Cha, G.-B.; Hong, S. C.; Kim, S.; Kim, J.; Jena, D.; Joo, J.; Kim, S. High-Detectivity Multilayer MoS_2 Phototransistors with Spectral Response from Ultraviolet to Infrared. *Adv. Mater.* **2012**, *24*, 5832–5836.
14. Lopez-Sanchez, O.; Lembke, D.; Kayci, M.; Radenovic, A.; Kis, A. Ultrasensitive Photodetectors Based on Monolayer MoS_2. *Nat. Nanotechnol.* **2013**, *8*, 497–501.
15. Tsai, D.-S.; Liu, K.-K.; Lien, D.-H.; Tsai, M.-L.; Kang, C.-F.; Lin, C.-A.; Li, L.-J.; He, J.-H. Few-Layer MoS_2 with High Broadband Photogain and Fast Optical Switching for Use in Harsh Environments. *ACS Nano* **2013**, *7*, 3905–3911.
16. Lee, H. S.; Min, S.-W.; Chang, Y.-G.; Park, M. K.; Nam, T.; Kim, H.; Kim, J. H.; Ryu, S.; Im, S. MoS_2 Nanosheet Phototransistors with Thickness-Modulated Optical Energy Gap. *Nano Lett.* **2012**, *12*, 3695–3700.
17. Buscema, M.; Barkelid, M.; Zwiller, V.; van der Zant, H. S. J.; Steele, G. A.; Castellanos-Gomez, A. Large and Tunable Photothermoelectric Effect in Single-Layer MoS_2. *Nano Lett.* **2013**, *13*, 358–363.
18. Wu, C.-C.; Jariwala, D.; Sangwan, V. K.; Marks, T. J.; Hersam, M. C.; Lauhon, L. J. Elucidating the Photoresponse of Ultrathin MoS_2 Field-Effect Transistors by Scanning Photocurrent Microscopy. *J. Phys. Chem. Lett.* **2013**, *4*, 2508–2513.
19. Monroy, E.; Omnès, F.; Calle, F. Wide-Bandgap Semiconductor Ultraviolet Photodetectors. *Semicond. Sci. Technol.* **2003**, *18*, R33–R51.
20. Das, S.; Chen, H.; Penumatcha, A. V.; Appenzeller, J. High Performance Multilayer MoS_2 Transistors with Scandium Contacts. *Nano Lett.* **2013**, *13*, 100–105.
21. Chuang, S.; Battaglia, C.; Azcat, A.; McDonnell, S.; Kang, J. S.; Yin, X.; Tosun, M.; Kapadia, R.; Fang, H.; Wallace, R. M.; Javey, A. MoS_2 P-type Transistors and Diodes Enabled by High Work Function MoO_x Contacts. *Nano Lett.* **2014**, *14*, 1337–1342.
22. Huang, J.-K.; Pu, J.; Hsu, C.-L.; Chiu, M.-H.; Juang, Z.-Y.; Chang, Y.-H.; Chang, W.-H.; Iwasa, Y.; Takenobu, T.; Li, L.-J. Large-Area Synthesis of Highly Crystalline WSe_2 Monolayers and Device Applications. *ACS Nano* **2014**, *8*, 923–930.
23. Li, H.; Wu, J.; Huang, X.; Lu, G.; Yang, J.; Lu, X.; Xiong, Q.; Zhang, H. Rapid and Reliable Thickness Identification of Two-Dimensional Nanosheets Using Optical Microscopy. *ACS Nano* **2013**, *7*, 10344–10355.
24. Fang, H.; Chuang, S.; Chang, T. C.; Takei, K.; Takahashi, T.; Javey, A. High-Performance Single Layered WSe_2 p-FETs with Chemically Doped Contacts. *Nano Lett.* **2012**, *12*, 3788–3792.
25. Liu, W.; Kang, J.; Sarkar, D.; Khatami, Y.; Jena, D.; Banerjee, K. Role of Metal Contacts in Designing High-Performance Monolayer n-Type WSe_2 Field Effect Transistors. *Nano Lett.* **2013**, *13*, 1983–1990.

26. Chen, T.-Y.; Loan, P. T. K.; Hsu, C.-L.; Lee, Y.-H.; Wang, T.-W.; Wei, K.-H.; Lin, C.-T.; Li, L.-J. Label-Free Detection of DNA Hybridization Using Transistors Based on CVD Grown Graphene. *Biosens. Bioelectron.* **2013**, *41*, 103–109.

27. Zhao, Y.; Luo, X.; Li, H.; Zhang, J.; Araujo, P. T.; Gan, C. K.; Wu, J.; Zhang, H.; Quek, S. Y.; Dresselhaus, M. S.; Xiong, Q. H. Interlayer Breathing and Shear Modes in Few-Trilayer MoS_2 and WSe_2. *Nano Lett.* **2013**, *13*, 1007–1015.

28. Zeng, H.; Liu, G.-B.; Dai, J.; Yan, Y.; Zhu, B.; He, R.; Xie, L.; Xu, S.; Chen, X.; Yao, W.; Cui, X. Optical Signature of Symmetry Variations and Spin-Valley Coupling in Atomically Thin Tungsten Dichalcogenides. *Sci, Rep.* **2013**, *3*, 1608.

29. Sahin, H.; Tongay, S.; Horzum, S.; Fan, W.; Zhou, J.; Li, J.; Wu, J.; Peeters, F. M. Anomalous Raman Spectra and Thickness-Dependent Electronic Properties of WSe_2. *Phys. Rev. B* **2013**, *87*, 165409.

30. Zhao, W.; Ribeiro, R. M.; Toh, M.; Carvalho, A.; Kloc, C.; Castro Neto, A. H.; Eda, G. Origin of Indirect Optical Transitions in Few-Layer MoS_2, WS_2, and WSe_2. *Nano Lett.* **2013**, *13*, 5627–5634.

31. Luo, X.; Zhao, Y.; Zhang, J.; Toh, M.; Kloc, C.; Xiong, Q.; Quek, S. Y. Effects of Lower Symmetry and Dimensionality on Raman Spectra in Two-Dimensional WSe_2. *Phys. Rev. B* **2013**, *88*, 195313.

32. Zhao, W.; Ghorannevis, Z.; Chu, L.; Toh, M.; Kloc, C.; Tan, P.-H.; Eda, G. Evolution of Electronic Structure in Atomically Thin Sheets of WS_2 and WSe_2. *ACS Nano* **2013**, *7*, 791–797.

33. Das, S.; Chen, H.-Y.; Penumatcha, A. V.; Appenzeller, J. High Performance Multilayer MoS_2 Transistors with Scandium Contacts. *Nano Lett.* **2013**, *13*, 100–105.

34. Zhang, W.; Zhang, J.; Li, P.; Shen, X.; Zhang, Q.; Wu, J. The Effects of Contacts and Ambipolar Electrical Transport in Nitrogen Doped Multiwall Carbon Nanotubes. *Nanotechnology* **2008**, *19*, 085202.

35. Zhang, W.; Zhang, Q.; Wu, J. Time-Related Conversion of the Carbon Nanotube Field Effect Transistor. *Appl. Phys. Lett.* **2006**, *89*, 233507.

36. Soci, C.; Zhang, A.; Xiang, B.; Dayeh, S. A.; Aplin, D. P. R.; Park, J.; Bao, X. Y.; Lo, Y. H.; Wang, D. ZnO Nanowire UV Photodetectors with High Internal Gain. *Nano Lett.* **2007**, *7*, 10031009.

37. González-Posada, F.; Songmuang, R.; Den Hertog, M.; Monroy, E. Room-Temperature Photodetection Dynamics of Single GaN Nanowires. *Nano Lett.* **2012**, *12*, 172–176.

38. Yang, Q.; Guo, X.; Wang, W.; Zhang, Y.; Xu, S.; Lien, D. H.; Wang, Z. L. Enhancing Sensitivity of a Single ZnO Micro-/Nanowire Photodetector by Piezo-phototronic Effect. *ACS Nano* **2010**, *4*, 6285–6291.

39. Gong, X.; Tong, M.; Xia, Y.; Cai, W.; Moon, J. S.; Cao, Y.; Yu, G.; Shieh, C.-L.; Nilsson, B.; Heeger, A. J. High-Detectivity Polymer Photodetectors with Spectral Response from 300 to 1450 nm. *Science* **2009**, *325*, 1665–1667.

40. Manga, K. K.; Wang, J.; Lin, M.; Zhang, J.; Nesladek, M.; Nalla, V.; Ji, W.; Loh, K. P. High-Performance Broadband Photodetector Using Solution-Processible PbSe-TiO(2)-Graphene Hybrids. *Adv. Mater.* **2012**, *24*, 1697–1702.

41. Manga, K. K.; Wang, S.; Jaiswal, M.; Bao, Q.; Loh, K. P. High-Gain Graphene-Titanium Oxide Photoconductor Made from Inkjet Printable Ionic Solution. *Adv. Mater.* **2010**, *22*, 5265–5270.

42. Moazzami, K.; Murphy, T. E.; Phillips, J. D.; Cheung, M. C.-K.; Cartwright, A. N. Sub-Bandgap Photoconductivity in ZnO Epilayers and Extraction of Trap Density Spectra. *Semicond. Sci. Technol.* **2006**, *21*, 717.

43. Jin, Y.; Wang, J.; Sun, B.; Blakesley, J. C.; Greenham, N. C. Solution-Processed Ultraviolet Photodetectors Based on Colloidal ZnO Nanoparticles. *Nano Lett.* **2008**, *8*, 1649–1653.

44. Sze, S. M. *Physics of Semiconductor Devices*; Wiley: New York, 1981; p 281.

45. Fan, Z.; Lua, J. G. Electrical Properties of ZnO Nanowire Field Effect Transistors Characterized with Scanning Probes. *Appl. Phys. Lett.* **2005**, *86*, 032111.

46. Freitag, M.; Tsang, J. C.; Bol, A.; Yuan, D.; Liu, J.; Avouris, P. Imaging of the Schottky Barriers and Charge Depletion in Carbon Nanotube Transistors. *Nano Lett.* **2007**, *7*, 2037–2042.

47. Zhang, Z. Y.; Jin, C. H.; Liang, X. L.; Chen, Q.; Peng, L.-M. Current-Voltage Characteristics and Parameter Retrieval of Semiconducting Nanowires. *Appl. Phys. Lett.* **2006**, *88*, 073102.

48. Bachtold, A.; Fuhrer, M. S.; Plyasunov, S.; Forero, M.; Anderson, E. H.; Zettl, A.; McEuen, P. L. Scanned Probe Microscopy of Electronic Transport in Carbon Nanotubes. *Phys. Rev. Lett.* **2000**, *84*, 6082.

49. Léonard, F.; Tersoff, J. Novel Length Scales in Nanotube Devices. *Phys. Rev. Lett.* **1999**, *83*, 5174.

50. Zhou, J.; Gu, Y.; Hu, Y.; Mai, W.; Yeh, P.-H.; Bao, G.; Sood, A. K.; Polla, D. L.; Wang, Z. L. Gigantic Enhancement in Response and Reset Time of ZnO UV Nanosensor by Utilizing Schottky Contact and Surface Functionalization. *Appl. Phys. Lett.* **2009**, *94*, 191103.

51. Freitag, M.; Tsang, J. C.; Kirtley, J.; Carlsen, A.; Chen, J.; Troeman, A.; Hilgenkamp, H.; Avouris, P. Electrically Excited, Localized Infrared Emission from Single Carbon Nanotubes. *Nano Lett.* **2006**, *6*, 1425–1433.

52. Xu, X.; Gabor, N. M.; Alden, J. S.; Zande, A. M.; van der, M.; Paul, L. Photo-Thermoelectric Effect at a Graphene Interface Junction. *Nano Lett.* **2010**, *10*, 562–566.

53. Misewich, J. A.; Martel, R.; Avouris, P.; Tsang, J. C.; Heinze, S.; Tersoff, J. Electrically Induced Optical Emission from a Carbon Nanotube FET. *Science* **2003**, *300*, 783–786.